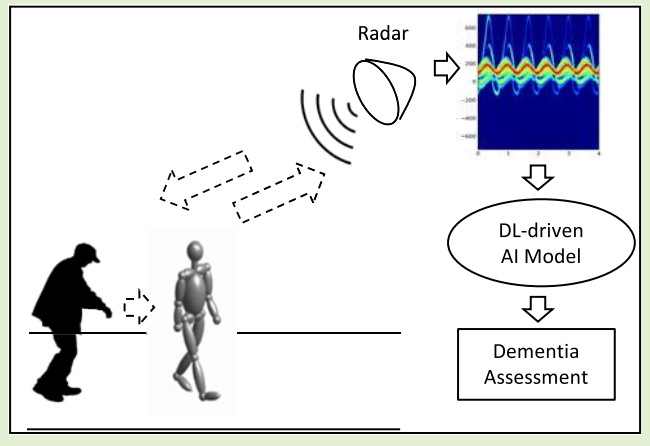


STRIDE: Systematic Radar Intelligence Analysis for ADRD Risk Evaluation With Gait Signature Simulation and Deep Learning

Fulin Cai[®], Abhidnya Patharkar[®], Teresa Wu[®], *Senior Member, IEEE*, Fleming Y. M. Lure, Harry Chen, and Victor C. Chen, *Life Fellow, IEEE*

Abstract—Abnormal gait is a significant noncognitive biomarker for Alzheimer's disease (AD) and AD-related dementia (ADRD). Micro-Doppler radar (MDR), a nonwearable technology, can capture human gait movements for potential early ADRD risk assessment. In this article, we propose to design a systematic radar intelligence analysis for ARDR risk evaluation (STRIDE) integrating MDR sensors with advanced artificial intelligence (AI) technologies. STRIDE embeds a new deep learning (DL) classification framework. As a proof of concept, we develop a "digital twin" of STRIDE, consisting of a human walking simulation model and an MDR simulation model, to generate a gait signature dataset. Taking established human walking parameters, the walking model simulates individuals with ADRD under various conditions. The radar model based on electromagnetic scattering and the Doppler frequency shift model is employed to generate micro-Doppler signatures from different moving body parts



(e.g., foot, limb, joint, torso, and shoulder). A band-dependent DL framework is developed to predict ADRD risks. The experimental results demonstrate the effectiveness and feasibility of STRIDE for evaluating ADRD risk.

Index Terms— Alzheimer's disease and related dementia (ADRD), deep learning (DL), gait analysis, micro-Doppler radar (MDR).

I. INTRODUCTION

N ESTIMATED 6.5 million elderly people in USA currently have Alzheimer's disease (AD), and the number is expected to increase to 13.8 million in 2050 [1]. Neurological changes of AD and AD-related dementia (ADRD) may occur 10–20 years before clinical symptoms arise [2]. Thus, there is a growing consensus that treatment should target the disease in the early phases, ideally before clinical symptoms

Manuscript received 18 February 2023; revised 13 March 2023; accepted 14 March 2023. Date of publication 3 April 2023; date of current version 15 May 2023. This work was supported by the National Institute of Aging under Grant 2R42AG053149-02A1. The associate editor coordinating the review of this article and approving it for publication was Prof. Huang C. Lee. (Corresponding author: Teresa Wu.)

Fulin Cai, Abhidnya Patharkar, and Teresa Wu are with the School of Computing and Augmented Intelligence and the ASU-Mayo Center for Innovative Imaging, Arizona State University, Tempe, AZ 85287 USA (e-mail: fulin.cai@asu.edu; apathark@asu.edu; teresa.wu@asu.edu).

Fleming Y. M. Lure, Harry Chen, and Victor C. Chen are with MS Technologies Corporation, Rockville, MD 20580 USA (e-mail: fleming.lure@mstechnologies.com; harry.chen@mstechnologies.com; v.c.chen@poctechgroup.com).

Digital Object Identifier 10.1109/JSEN.2023.3263071

manifest. This relies on screening and early detection services to recognize significant biomarkers.

Abnormal gait is prevalent in established dementia [3], and human gaits shall be an effective biomarker associated with progression from normal cognition, cognitive complaints, and mild cognitive impairment (MCI) to dementia syndromes [4], [5], [6], [7], [8], [9]. In addition, gait variability can be observed ten years before clinical symptoms of ADRD [10]. Referenced as the "sixth vital sign" [11], gait parameters (e.g., speed, step/stride length, and step time/angle) have been quantitatively investigated for their association with cognitive performance [12]. Gait parameters have also been employed as a marker to support diagnosis among healthy elderly, MCI, and AD patients [13]. Given their importance, gait-related sensors are becoming increasingly necessary to capture motions and assist ADRD early diagnosis.

Radar, a nonwearable sensor (NWS) has been demonstrated to be effective in capturing object movements remotely [14], [15], [16], [17] and is also capable of detecting micromotion (e.g., vital signs) [18]. Unlike wearable sensors, NWS is not intrusive and does not require continuous wear

1558-1748 © 2023 IEEE. Personal use is permitted, but republication/redistribution requires IEEE permission. See https://www.ieee.org/publications/rights/index.html for more information.

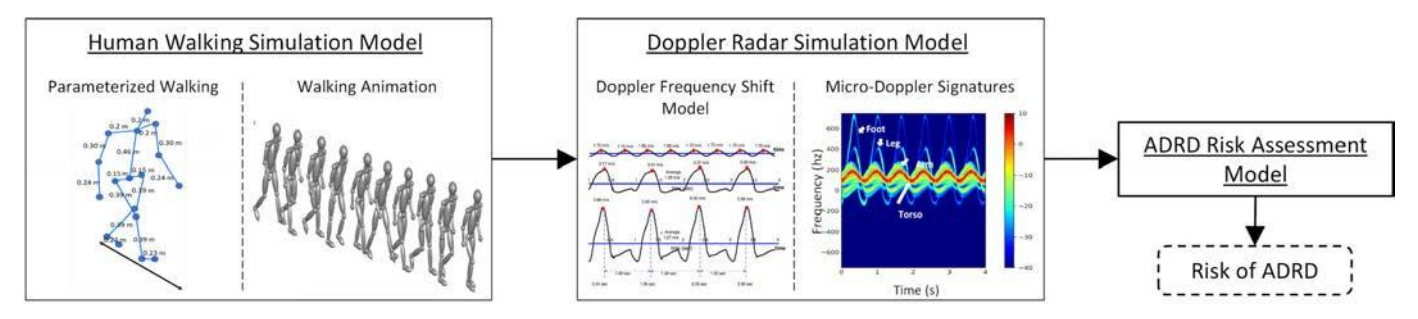


Fig. 1. Overview of STRIDE.

by the elderly. Other NWS systems, based on optoelectronic sensors or camera-based visual image sequences [3], are subject to various issues. For example, it can be easily affected by the distance of the human subject from the sensor, variations in lighting, background complexity, deformations caused by human clothing, or some coverings on the human subject. In addition, privacy concerns are often raised when camera-based sensors record plain images of the subject or environment. In several studies, micro-Doppler radar (MDR) is effective for capturing gait motion by utilizing the Doppler effect to only reflect movements [18], [19], [20], [21], [22], [23].

Gait motions during walking are monitored by MDR and transformed into micro-Doppler signatures. These signatures are then represented on a time–frequency image such as a spectrogram. Gait features, then, are estimated for MCI recognition [24], [25], [26] and dementia diagnosis [27]. Typically, leg motions derived from upper and lower envelopes on a spectrogram are proven to be distinctive features [24], [25], [26]. Artificial intelligence (AI), mostly machine learning (ML), plays a critical role in bridging the gap between estimated gait parameters and cognitive impairment.

Admittedly, ML-based applications are effective in correlating gait parameters with dementia, and their prediction performances are promising. However, the potential of deep learning (DL), a prevalent research branch of AI, has yet to be fully explored for the evaluation of ADRD risk. Unlike ML, DL models the relationship between inputs and outputs and learns to identify effective features through end-to-end training [28]. In addition, DL has shown outperformance over ML in radar sensing applications [23], [29], [30], [31].

In this study, we propose a systematic radar intelligence analysis for ARDR risk evaluation (STRIDE) with gait signature simulation and DL. The STRIDE integrates MDR sensors to capture human gait signatures and assess the level of gait impairment associated with ADRD risk levels, with the assistance of DL models. A large gait signature dataset is essential for implementing DL models. However, there is no publicly available gait dataset related to ARRD risk evaluation, to the best of our knowledge. To conduct a pilot test of the concept, we develop the "digital twin" of STRIDE, including a human walking simulator and an MDR simulator to address the absence of gait data about dementia. This article has three contributions.

- 1) STRIDE, an integrated system for ADRD risk assessment with potential clinical utility is proposed.
- 2) To validate the effectiveness and feasibility of the system for ADRD studies, a "digital twin" is designed and implemented for gait signature generation.
- 3) A novel DL framework, named band-dependent learning (BDL), is developed to automatically assess the ADRD risk. Observing band-dependent patterns in radar spectrogram, BDL-ResNet is designed to capture the information effectively by identifying the salient subbands along frequency and time ranges.

This article is organized as follows. In Section II, the details of "digital twin" and BDL of STRIDE are provided followed by the experiments in Section III. The conclusion and future work are discussed in Section IV.

II. AUTOMATIC ADRD RISK EVALUATION SYSTEM—RADAR SCENARIO, GAIT SIMULATION, AND LEARNING MODEL

An overview of STRIDE is shown in Fig. 1. STRIDE consists of: 1) a human walking simulation model using the parameters collected from the literature; 2) an MDR simulation model to monitor animated human walking; and 3) a DL framework for ADRD risk assessment.

A. Human Walking Simulation Model

Human gait, which reflects the manner of human walking, has been studied for decades in biomedical engineering, sports medicine, physiotherapy, medical diagnosis, and rehabilitation [3], [32], [33], [34]. Human walk is a highly coordinated periodic movement involving the brain, muscles, nerves, joints, and bones [35], [36]. It has been observed that the gait features of individuals with memory and cognitive dysfunctions are different from those of healthy individuals [33], [37]. Also, the severity of dementia may correlate with the presence of gait abnormalities [38].

Clinical literature indicates that elderly individuals with dementia may exhibit lower walking speed, shorter step length, imbalanced steps, and longer stance phases compared to healthy elderly people [38]. In addition, individuals with severe abnormalities may walk with head and neck bent over, with drag, drop, or shuffle feet, or with irregular or jerky walking. Thus, analyzing gait features shall help capture and even predict possible cognitive decline. Despite the

Parameters	Normal Walk	Subtle Abnormality Walk	Moderate Abnormality Walk	Severe Abnormality Walk
Height (m)	[1.6, 1.8]	[1.6, 1.8]	[1.6, 1.8]	[1.6, 1.8]
Walking Speed (m/s)	0.6	0.6	0.6	0.5
Durations of Walk Cycle (s)	[1.54, 1.63]	[1.54, 1.63]	[1.54, 1.63]	[1.69, 1.79]
Duration of Support (s)	[1.02, 1.09]	[1.06, 1.12]	[1.06, 1.12]	[1.23, 1.30]
Duration of Balance(s)	[0.52, 0.55]	[0.48, 0.51]	[0.48, 0.51]	[0.46, 0.49]
Duration of Double Support (s)	[0.25, 0.27]	[0.27, 0.28]	[0.27, 0.28]	[0.34, 0.37]
Percentage of Support Duration	65.9%	68.8%	69.0%	72.9%

TABLE I
PARAMETERS OF WALKING WITH DIFFERENT ADRD RISK LEVELS

extensive literature on the use of gait features in supporting the diagnosis of memory and cognitive dysfunctions [4], [10], [39], [40], [41], [42], [43], [44], existing gait datasets are limited to young, healthy individuals and collected in a clinical/laboratory setting. A large, publicly available dataset for gait abnormality analysis is currently lacking.

To address the challenge, we propose to develop a human walking simulation model for various ADRD risk levels. Human gait can be decomposed into periodic motions in a gait cycle. One cycle consists of two phases: the stance (or support) phase and the swing phase [35]. During the stance phase, the foot is on the ground with a heel strike and a toe-off. In the swing phase, the foot is lifted from the ground with acceleration or deceleration. Key parameters used to describe a complete walking gait include walking speed, step length, and stance time, with associated variances. The walking cycle is also divided into three durations: the duration of single support, the duration of balance, and the duration of double support characterized based on the contact of the feet with the ground [35].

We develop a simulated walking model based on the well-validated global walking model [45], [46]. Using the parameters collected from literature depicting elderly gait patterns (see Table I), the human walking simulation model generates a large number of experimental human gait data with various spatial and temporal characteristics in the 3-D space. The MATLAB source code is provided in [45].

The global walking model presents the gait motion by 3-D trajectories of a walking human body over time. Specifically, one cycle of gait motion is described by three translations and 14 rotations (four body rotations and ten body parts rotations). The translations and rotations depend on walking speed, which can be derived from biomechanical experimental data [45], [47]. Based on the translations and the rotations, 12 3-D translational trajectories are obtained. The positions of the 17 joint points at each time frame are derived from the 3-D trajectories using the Euler angle rotation matrix [45]. The joint motions in the 3-D space are used to deduce the movements of human body parts, such as head, torso, shoulders, arms, hips, legs, and feet. It is worth noting that the linear and angular kinematic parameters are further used to calculate radar returns caused by the walking motions (see Section II-B).

Table I summarizes the parameters used in the model under four different ADRD conditions. As aforementioned, a walking cycle consists of the duration of support, balance, and

double support. These durations are related to the duration of walking cycle, which is influenced by the height and the walking speed. They are used to derive the motion of the joints. In this study, we assume an elderly with height, from H = 1.601.80 m, and walking speed, V = 0.6 m/s [38]. According to [45] and [47], we get the following parameters.

- 1) The relative speed is rescaled by the height of the leg, $R_V = V/(H/2) \approx 0.68-0.76$.
- 2) For a normal walking cycle, the duration of a walking cycle is determined by $D_c = (1.346/(Rv)^{1/2}) \approx 1.541.63$ s.
- 3) The duration of support is $D_s = 0.762 \times D_c 0.143 \approx 1.021.09$ s.
- 4) The duration of balance is $D_b = 0.248 \times D_c + 0.143 \approx 0.52 0.55$ s.
- 5) The duration of double support is $D_{ds} = 0.252 \times D_c 0.143 \approx 0.250.27$ s. Note that $D_c = D_s + D_b$.

Compared to normal walking, the elderly abnormal walking has a longer duration of stance, i.e., 60%–75% of the duration of the walking cycle, leading to longer support duration. According to [38], we summarize the percentage of support duration $P_{\rm sd}$ for each category in Table I. D_s , D_b , and D_{ds} are given as follows:

$$D_s = P_{\rm sd} (1 + 0.15 \times \text{rand}) \times D_c \tag{1}$$

$$D_b = D_c - D_s \tag{2}$$

$$D_{ds} = 0.25 \times D_s \tag{3}$$

where rand is a random number within [0, 1].

B. Doppler Radar Simulation Model

MDR is effective in detecting micromotions—humans periodically swing their arms and legs and move the body's center of gravity up and down [35], [45]. The global walking speed can also be inferred from the motions captured by MDR [19]. MDR devices have been utilized to observe the walking process and produce the corresponding micro-Doppler signatures for gait analysis [19], [21].

In our case, a Doppler radar simulation model is developed to detect walking motions on the virtual path [45]. The radar is located at the end of the path (e.g., X_1 = 10 m, Y_1 = 0 m, and Z_1 = 1 m) and the starting point of human walking is located at (X_0 = 0, Y_0 = 0, and Z_0 = 0). Once the walking (Section II-A) starts, a frequency-modulated continuous-wave (FMCW) radar is simulated to periodically transmit and receive signals until the walking simulation ends.

According to [45], the Doppler frequency shift $f_{D,k}$, induced by motions of human bodies during the walking process, is calculated as

$$f_{D,k} = -\left(2f_c/c\right)v_k\cos\theta_k\tag{4}$$

where c is the wave propagation speed, f_c is the radar carrier frequency, v_k is the velocity of the kth body part, and θ_k is the corresponding line-of-sight angle between the radar and the kth body part. For the FMCW radar, the Doppler resolution and the range resolution are computed, respectively, by

$$\Delta f_D = 1/(nT_{\rm sw}) \tag{5}$$

$$\Delta R = c / (2\Delta B) \tag{6}$$

where n is the number of group sweeps, T_{sw} is the sweep time, and ΔB is the bandwidth of the signal [45].

In this study, the bandwidth of the radar is 1.5 GHz, the sweep time is 1.0 ms, and the number of group sweeps is 512. Therefore, the simulated MDR has 0.1 m range resolution and 1.95 GHz Doppler resolution. The received signals are transformed into micro-Doppler signatures on a spectrogram through the short-time Fourier transform (STFT) [48].

C. Band-Dependent Deep Learning Model for ADRD Risk Assessment

The spectrogram, which contains micro-Doppler signatures of walking (see Fig. 1), is a one-channel time-frequency image. Recently, DL has made great success in image studies, including time-frequency images [23], [28], [49], [50]. Unlike the natural image, the spectrogram represents a signal in a view of both time and frequency. It shows the variation in the frequency domain and does not satisfy the translation invariance [51]. In addition, as frequency increases, the power of the reflected signal decreases. Therefore, considering a certain frequency range as a subband, time-frequency spectrogram often has band-dependent patterns observed.

Several studies have adopted convolutional networks on subbands by limiting the kernel sharing or customizing the kernel scale [50], [51], [52], [53]. The issue with such an approach is that it requires extensive computation and memory to run multiple network models in parallel. To dedicate one network model for each subband, Chang et al. [54] proposed a shared network and developed a band-level normalization to adjust the imbalanced scales between the subbands. However, in our study, such normalization may face serious challenges from the high-frequency band where the power of the noise is similar to that of the signal reflecting from the body parts such as feet and legs (see Fig. 2).

To address this issue, we propose a BDL framework to divide the spectrogram and fuse the diverse representations of subbands. The framework leverages the generalization capabilities of vision models such as ResNet-18 [55] and separately identifies representations in each subband. The obtained representations (feature vectors) are then normalized to reduce the scale difference between subbands and selectively combined to balance the contribution of each subband using a learnable weight vector.

The workflow of the BDL framework is shown in Fig. 3. The input spectrogram is first equally partitioned into Nnonoverlapping subbands with the output feature vectors depicting the characteristics of the subbands. This way ensures that the features of each band are captured fairly. The feature vectors are then normalized to be on the unit hypersphere so that the scale difference between subbands can be mitigated. Next, the feature vectors are concatenated and multiplied by a learnable weight vector whose dimension corresponds to the number of subbands. This vector is used to fuse the N feature vectors to adjust the contributions from the subbands on the final feature vector. Before the multiplication, the elements of the weight vector are mapped to [0, 1] by the sigmoid function. Hence, the elements of the weight vector are initialized to 0. The weighted feature vector is used in a classifier for the final prediction.

III. EXPERIMENTS

The human walking simulator generates four types of walks for ADRD risks: normal, subtle abnormality, moderate abnormality, and severe abnormality. The parameters are randomly selected within the ranges specified in Table I. In this study, 2000 walks for each category are generated, resulting in a total of 8000 samples. These walking animations are presented on a simulated 10 m walking path under the detection of the Doppler radar. -15 dBm adaptive weight Gaussian noise (AWGN) is added to the channel to mimic the real-world scenario. The radar records approximately a 4-s walking period and transforms all collected signals into MDR signatures on a spectrogram by STFT. For STFT, the number of discrete Fourier transform (DFT) points is 512 and there are 256 overlapped samples for each window. The Kaiser window with 256 points is employed. Each spectrogram thus has a one-channel time-frequency image with 512 and 776 dimensions for the frequency and time domains, respectively.

Spectrograms are preprocessed by applying $x = 20 \times \log_{10}(x + 1e^{-5})$ to each data point x. This function can magnify the low-power data points, which might be the signatures of the foot and the leg. Fig. 2 shows the example micro-Doppler signatures of the four ADRD risk levels under the noisy scenario. Most of the signatures appear in the positive frequency and a few in the negative frequency because human arms and hips periodically move forward and backward while walking. In addition, most of the signatures of the joint occur within [-100, 300] Hz. The signatures of feet and legs, which have faster moving speeds, appear in the whole positive frequency. However, the signals are shadowed by the noises and become blurred in the high-frequency range.

To verify the performance of the ADRD risk assessment model (BDL-ResNet), the 8000 samples are divided into a training set (70%), a validation set (15%), and a test set (15%). For comparison, two DL models (GoogleNet [56] and ResNet-18 [55]) and two ML models [24], [27] are implemented as benchmarks. The DL models are fine-tuned on the training set and they tend to focus on the entire frequency domain for representation learning. Please note that the one-channel spectrogram is replicated three times to fit the input requirement (three channels) of the DL vision models. The

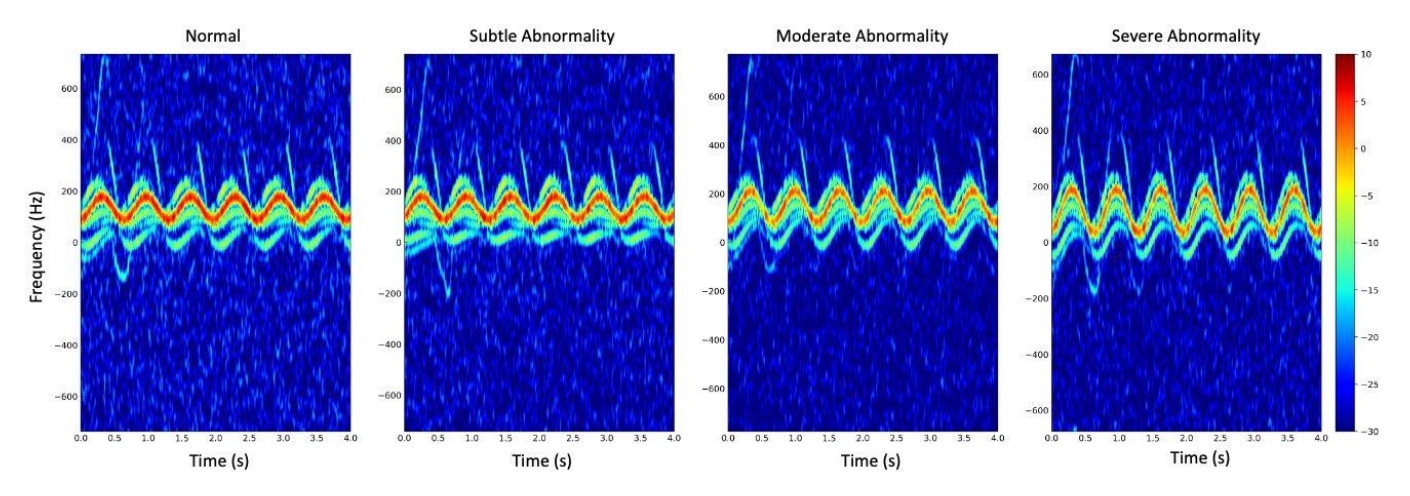


Fig. 2. Plots of samples of micro-Doppler signatures with different ADRD risk levels under noisy environment.

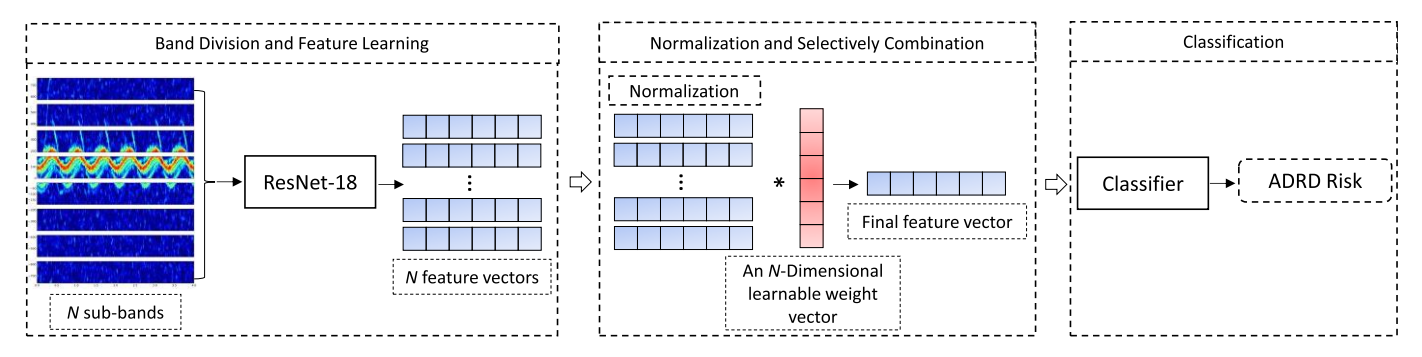


Fig. 3. Overview of the BDL framework.

two ML models extract gait-related features and use support vector machine (SVM) [24] and neural network (NN) [27] as the classifier.

For the parameter settings, the output from ResNet-18 is a 512-D feature vector. The classifier of BDL-ResNet is a 512 by four one-layer fully connected network using the rectified linear unit (ReLu) activation and the batch normalization. All experiments use the cross entropy as the loss function and 64 as the batch size. For the weight vector, $2e^{-1}$ is employed for faster convergence. We set the learning rate to $1e^{-3}$ for all DL models and train them up to five epochs using the Adam optimizer [57]. The training process is early stopped based on the validation results. For the ML models, all settings are as specified in the original references.

To fully compare the performance of the algorithms, we use accuracy for overall evaluation. Precision and sensitivity are for class-wise evaluation. The metrics are defined as follows:

Accuracy = # of correct predictions/total # of samples

$$Precision = TP/(TP + FP)$$
 (8)

Sensitivity =
$$TP/(TP + FN)$$
 (9)

where TP, FP, and FN are the true positive samples, false positive samples, and false negative samples, respectively. These three variables are evaluated in a class-specific manner [58].

First, to determine the number of subbands, N, we conduct experiments training the models using N from 2, 4, 8, to 16

TABLE II
Validation Results of N

N	Accuracy on Validation Set
2	0.906
4	0.913
8	0.922
16	0.922

and test them on the validation set for comparison. The accuracy results are summarized in Table II. The validation results indicate that the model performs well for N being 8 and 16. We decide to set N to 8 considering the computation efficiency. The result that the accuracy increases with N also demonstrates the advantages of subband-based studies.

Next, BDL-ResNet (N=8) is compared with the other four algorithms in overall and class-wise evaluations on the test set. To evaluate the robustness of the method, the experiments are repeated 30 times. Please note that the dataset is resplit and the models are reinitialized in each run. The means and standard deviations of the four metrics are calculated. We conduct the one-sided t-test using the results of the 30 runs. It can be concluded that BDL-ResNet is statistically greater than the competitor when the p-value is less than 0.05.

As summarized in Table III, BDL-ResNet significantly outperforms the other algorithms in terms of overall accuracy with at least 95% confidence. Both DL vision models provide competitive performance for ADRD risk evaluation, while ML_NN

TABLE III

OVERALL PERFORMANCE STATISTICS ON THE TEST SET

	Accuracy			
Algorithm	$Mean \pm Std$	<i>p</i> -value (BDL-ResNet vs.)		
ML_SVM [24]	0.898 ± 0.007	0.000		
ML_NN [27]	0.740 ± 0.007	0.000		
GoogleNet	0.905 ± 0.013	0.000		
ResNet-18	0.884 ± 0.078	0.012		
BDL-ResNet	0.923 ± 0.018	~		

only achieves 74% overall accuracy. The BDL framework significantly improves the performance of ResNet according to the result (0.923 \pm 0.018 versus 0.884 \pm 0.078 and p=0.012). This improvement indicates the advantage of BDL, which reduces the impact of variability among frequencies and emphasizes the salient subbands.

The class-wise performance results are presented in Table IV. For the normal and subtle abnormality groups, our method performs the best with at least 95% confidence in terms of precision and is comparable to the best candidates for sensitivity. Specifically, for the normal group, BDL-ResNet outperforms ResNet-18 in precision (0.977 \pm 0.028 versus 0.877 ± 0.294 and p = 0.037) and sensitivity (0.996 \pm 0.009 versus 0.861 \pm 0.307 and p = 0.011). For the subtle abnormal walking group, BDL-ResNet outperforms ResNet-18 in terms of precision (0.822 \pm 0.035 versus 0.77 \pm 0.134 and p = 0.023) and obtains a comparable sensitivity result. This group is the most challenging to investigate and has the worst overall prediction performance among all four groups, but our method still outperforms ResNet-18 in categorizing subjects with subtle abnormalities, due to the benefits of the BDL framework. In addition, BDL-ResNet is statistically better than two ML models (0.750 \pm 0.002 and 0.577 \pm 0.027) in terms of precision to a large extent to detect the subtle abnormality. These results are desirable showing that our method can better categorize normal walking with fewer "false alarms" and more accurately detect subtle abnormality (early stage).

For the severe abnormality groups, all algorithms have excellent performance. This indicates the power of DL in general to support the study. For the moderate abnormality group, it is interesting to observe that our method exhibits comparable performance to other candidates. However, our method marginally underperforms in precision (0.920 \pm 0.072 versus 0.942 \pm 0.013 and p=0.945) and sensitivity (0.794 \pm 0.071 versus 0.805 \pm 0.072 and p=0.705) though no statistical conclusion can be drawn. It is our intention to improve our framework focusing on this group as the immediate next step.

To further shed light on the behavior of the model, we visualize the weights that the model places on each subband. Please note that the model uniformly splits the spectrogram into eight subbands. Fig. 4 shows the weight values and the corresponding body parts whose signatures appear in each subband. The trained model gives high importance, 0.96 and 0.86, to the third subband and the fourth subband, respectively. The results indicate that the model underscores these two

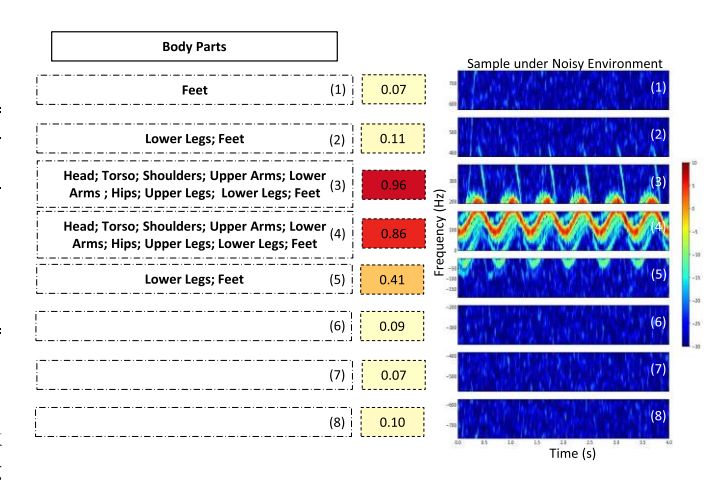


Fig. 4. Plots of weights on eight subbands. Left: body parts whose signatures occur in the subband. Right: spectrogram sample with band division (N = 8).

subbands, which contain the signatures of all body parts. The third band contains the clear signatures of the legs' movements, whereas the fourth band contains the overlapping signatures of all body parts. The legs' signatures strongly correlate to the walking dysfunction caused by ADRD [8]. The signatures in the fifth band have a lower importance rate (0.41), despite being related to movements of the feet and the legs. These signatures correspond to the duration of double support when both feet are in contact with the ground and the legs are together. Hence, the differences between categories are less discriminative in this subband. Although the first two subbands have the signatures of the feet and the legs, the power of the signatures is relatively low. Their shapes become blurred as they are shadowed by the noise. In addition, the last three bands are uninformative ranges (the last three bands), which have no micro-Doppler signature. The model can recognize these facts and pays nearly zero attention to those subbands. These results verify our proposed model and motivate our future work to interrogate the clinical implications focusing on the signatures from important subbands.

IV. DISCUSSION

Referring to dementia-related gait parameters, the "digital twin" can produce adequate gait signatures for four different ADRD risk levels to validate the concept of STRIDE. The ADRD risk assessment model is built upon the novel BDL framework, where the scale difference among subbands is normalized in a high-level feature space and the significant subband is augmented in the decision-making of the classifier. Benefiting from this advantage, BDL-ResNet demonstrates its superiority compared to the four state-of-the-art (SOTA) models according to the results of the overall evaluation (accuracy), as well as the class-wise evaluations (precision and sensitivity). In addition, since the competitive performances on the normal and subtle abnormality groups, we conclude that our method has great potential to be an early detection tool for ADRD assessment.

In future work, we plan to address the following limitations. First, it can be challenging to classify subjects of the subtle and moderate abnormality groups. We thus plan

Class-wise Evaluation	Algorithm	Precision		Sensitivity	
		$Mean \pm Std$	<i>p</i> -value (BDL-ResNet vs.)	$Mean \pm Std$	<i>p</i> -value (BDL- ResNet vs.)
Normal	ML_SVM [24] ML_NN [27] GoogleNet ResNet-18 BDL-ResNet	0.942 ± 0.010 0.673 ± 0.024 0.966 ± 0.024 0.877 ± 0.294 0.977 ± 0.028	0.000 0.000 0.006 0.037	0.989 ± 0.005 0.823 ± 0.055 0.996 ± 0.001 0.861 ± 0.307 0.996 ± 0.009	0.000 0.000 0.484 0.011
Subtle Abnormality	ML_SVM [24] ML_NN [27] GoogleNet ResNet-18 BDL-ResNet	$0.750 \pm 0.002 \\ 0.577 \pm 0.027 \\ 0.769 \pm 0.028 \\ 0.770 \pm 0.134 \\ \textbf{0.822} \pm \textbf{0.035}$	0.000 0.000 0.000 0.000 0.023	$\begin{array}{c} \textbf{0.908} \pm \textbf{0.016} \\ 0.578 \pm 0.057 \\ 0.899 \pm 0.080 \\ 0.876 \pm 0.135 \\ \textbf{0.902} \pm \textbf{0.087} \end{array}$	0.632 0.000 0.435 0.191
Moderate Abnormality	ML_SVM [24] ML_NN [27] GoogleNet ResNet BDL-ResNet	$\begin{array}{c} \textbf{0.942} \pm \textbf{0.013} \\ 0.775 \pm 0.040 \\ \textbf{0.920} \pm \textbf{0.064} \\ 0.899 \pm 0.101 \\ \textbf{0.920} \pm \textbf{0.072} \end{array}$	0.945 0.000 0.502 0.176	0.696 ± 0.030 0.586 ± 0.045 0.723 ± 0.059 0.805 ± 0.072 0.794 ± 0.071	0.000 0.000 0.000 0.705
Severe Abnormality	ML_SVM [24] ML_NN [27] GoogleNet ResNet BDL-ResNet	$\begin{array}{c} \textbf{1.000} \pm \textbf{0.000} \\ 0.966 \pm 0.018 \\ \textbf{0.998} \pm \textbf{0.005} \\ \textbf{0.997} \pm \textbf{0.013} \\ \textbf{0.995} \pm \textbf{0.014} \end{array}$	0.962 0.000 0.892 0.723	$ \begin{aligned} & \textbf{1.000} \pm \textbf{0.000} \\ & 0.971 \pm 0.013 \\ & \textbf{0.999} \pm \textbf{0.002} \\ & \textbf{0.996} \pm \textbf{0.015} \\ & \textbf{0.997} \pm \textbf{0.014} \end{aligned} $	0.893 0.000 0.856 0.398

TABLE IV
CLASS-WISE PERFORMANCE STATISTICS ON THE TEST SET

to include focal loss or sampling methods, so the model would concentrate more on these easily misclassified samples. In addition, the number of subbands used in the framework is currently determined by the validation. We plan to develop a trainable band division model to adaptively divide the original spectrogram into several high inter- and low intra-difference subbands. It is also important to note that the simulation scenario of STRIDE is close to an empty experiment room with channel noise, which is not a realistic case. Interference from clutter and multisubjects should be further included in the simulation to mimic a daily living scenario. Other than these factors, an elderly specific human model is expected to analyze the characteristics of elderly people, such as humpback and tremors. In addition, MDR sensors have been used in-bed monitoring for vital signs in the hospital. It is our intention to explore the applicability of STRIDE in a real living context and clinics for field testing. We plan to explore transfer learning techniques to adapt the trained DL model of STRIDE to real-world data.

V. CONCLUSION

In this article, we proposed STRIDE, systematic radar intelligence analysis for ADRD risk evaluation, as a potential clinical tool. To validate the concept, we developed a "digital twin" of STRIDE and a novel DL framework focusing on frequency BDL ability. We generated a valid gait signature dataset categorized according to the ADRD risk level and then conducted comprehensive experiments to evaluate the effectiveness of the proposed DL model for ADRD risk assessment. Experimental results supported the effectiveness and feasibility of the system in terms of the quality of the ADRD risk assessment. In addition, we leveraged the learned weight vector for clinical interpretation.

ACKNOWLEDGMENT

The U.S. Government is authorized to reproduce and distribute for governmental purposes notwithstanding any copyright annotation of the work by the author(s). The views and conclusions contained herein are those of the authors and should not be interpreted as necessarily representing the official policies or endorsements, either expressed or implied, of NIH, Bethesda, MD, USA, or the U.S. Government.

REFERENCES

- [1] Alzheimer's Association, "2022 Alzheimer's disease facts and figures," *Alzheimer's Dement.*, vol. 18, no. 4, pp. 700–789, 2022. [Online]. Available: https://pubmed.ncbi.nlm.nih.gov/35289055/
- [2] R. J. Bateman, R. J. Bateman, and C. Xiong, "Clinical and biomarker changes in dominantly inherited Alzheimer's disease," *New England J. Med.*, vol. 367, pp. 795–804, Sep. 2012.
- [3] A. Muro-De-La-Herran, B. Garcia-Zapirain, and A. Mendez-Zorrilla, "Gait analysis methods: An overview of wearable and non-wearable systems, highlighting clinical applications," *Sensors*, vol. 14, no. 2, pp. 3362–3394, 2014.
- [4] J. Verghese, R. B. Lipton, C. B. Hall, G. Kuslansky, M. J. Katz, and H. Buschke, "Abnormality of gait as a predictor of non-Alzheimer's dementia," *New Eng. J. Med.*, vol. 347, no. 22, pp. 1761–1768, 2002.
- [5] J. K. Kueper, M. Speechley, N. R. Lingum, and M. Montero-Odasso, "Motor function and incident dementia: A systematic review and metaanalysis," *Age Ageing*, vol. 46, no. 5, pp. 729–738, Sep. 2017.
- [6] J. Verghese et al., "Motoric cognitive risk syndrome: Multicountry prevalence and dementia risk," *Neurology*, vol. 83, no. 8, pp. 718–726, Aug. 2014.
- [7] R. Savica et al., "Comparison of gait parameters for predicting cognitive decline: The mayo clinic study of aging," *J. Alzheimer's Disease*, vol. 55, no. 2, pp. 559–567, Nov. 2016.
- [8] M. Montero-Odasso et al., "CCCDTD5 recommendations on early non cognitive markers of dementia: A Canadian consensus," *Alzheimer's Dementia, Transl. Res. Clin. Intervent.*, vol. 6, no. 1, Jan. 2020, Art. no. e12068.
- [9] M. M. Montero-Odasso et al., "Association of dual-task gait with incident dementia in mild cognitive impairment: Results from the gait and brain study," *JAMA Neurol.*, vol. 74, no. 7, pp. 857–865, 2017.

- [10] P. Mahlknecht et al., "Prevalence and burden of gait disorders in elderly men and women aged 60–97 years: A population-based study," *PLoS ONE*, vol. 8, no. 7, Jul. 2013, Art. no. e69627.
- [11] S. Fritz and M. Lusardi, "White paper: 'Walking speed: The sixth vital sign," *J. Geriatric Phys. Therapy*, vol. 32, no. 2, pp. 2–5, 2009.
- [12] J. Verghese, C. Wang, R. B. Lipton, R. Holtzer, and X. Xue, "Quantitative gait dysfunction and risk of cognitive decline and dementia," J. Neurol. Neurosurg. Psychiatry, vol. 78, no. 9, pp. 929–935, Sep. 2007.
- [13] F. D. O. Silva et al., "Gait analysis with videogrammetry can differentiate healthy elderly, mild cognitive impairment, and Alzheimer's disease: A cross-sectional study," *Experim. Gerontology*, vol. 131, Mar. 2020, Art. no. 110816.
- [14] X. Xu, X. Zhang, T. Zhang, Z. Yang, J. Shi, and X. Zhan, "Shadow-background-noise 3D spatial decomposition using sparse low-rank Gaussian properties for video-SAR moving target shadow enhancement," *IEEE Geosci. Remote Sens. Lett.*, vol. 19, pp. 1–5, 2022.
- [15] T. Zhang and X. Zhang, "A mask attention interaction and scale enhancement network for SAR ship instance segmentation," *IEEE Geosci. Remote Sens. Lett.*, vol. 19, pp. 1–5, 2022.
- [16] X. Xu et al., "A group-wise feature enhancement-and-fusion network with dual-polarization feature enrichment for SAR ship detection," *Remote Sens.*, vol. 14, no. 20, p. 5276, 2022, doi: 10.3390/rs14205276.
- [17] T. Zhang, X. Zhang, J. Shi, and S. Wei, "Depthwise separable convolution neural network for high-speed SAR ship detection," *Remote Sens.*, vol. 11, no. 21, p. 2483, 2019, doi: 10.3390/rs11212483.
- [18] D. F. Fioranelli, D. S. A. Shah, H. Li, A. Shrestha, D. S. Yang, and D. J. Le Kernec, "Radar sensing for healthcare," *Electron. Lett.*, vol. 55, no. 19, pp. 1022–1024, 2019.
- [19] S. L. Mancini, W. Troy, K. A. Hall, X. Wu, and H. Wang, "Radar technology as a mechanism for clinical gait analysis: A review," *J. Ann. Bioeng.*, vol. 2021, no. 1, pp. 151–158, Jan. 2021.
- [20] H. Abedi, J. Boger, P. P. Morita, A. Wong, and G. Shaker, "Hall-way gait monitoring using novel radar signal processing and unsupervised learning," *IEEE Sensors J.*, vol. 22, no. 15, pp. 15133–15145, Aug. 2022.
- [21] A.-K. Seifert, M. Grimmer, and A. M. Zoubir, "Doppler radar for the extraction of biomechanical parameters in gait analysis," *IEEE J. Biomed. Health Informat.*, vol. 25, no. 2, pp. 547–558, Feb. 2021.
- [22] J. E. Kiriazi, O. Boric-Lubecke, and V. M. Lubecke, "Dual-frequency technique for assessment of cardiopulmonary effective RCS and displacement," *IEEE Sensors J.*, vol. 12, no. 3, pp. 574–582, Mar. 2012.
- [23] S. Z. Gurbuz and M. G. Amin, "Radar-based human-motion recognition with deep learning: Promising applications for indoor monitoring," *IEEE Signal Process. Mag.*, vol. 36, no. 4, pp. 16–28, Jul. 2019.
- [24] K. Saho, K. Uemura, K. Sugano, and M. Matsumoto, "Using micro-Doppler radar to measure gait features associated with cognitive functions in elderly adults," *IEEE Access*, vol. 7, pp. 24122–24131, 2019.
- [25] K. Saho, K. Uemura, and M. Matsumoto, "Screening of mild cognitive impairment in elderly via Doppler radar gait measurement," *IEICE Commun. Exp.*, vol. 9, no. 1, pp. 19–24, 2020.
- [26] K. Saho, K. Sugano, M. Kita, K. Uemura, and M. Matsumoto, "Classification of health literacy and cognitive impairments using higher-order kinematic parameters of the sit-to-stand movement from a monostatic Doppler radar," *IEEE Sensors J.*, vol. 21, no. 8, pp. 10183–10192, Apr. 2021.
- [27] R. Ishibashi, N. Nojiri, K. Saho, and L. Meng, "Dementia diagnose based on machine learning using Doppler radar image for the elderly person," in *Proc. 4th Int. Symp. Adv. Technol. Appl. Internet Things* (ATAIT), vol. 3198, 2022, pp. 17–24.
- [28] Y. LeCun, Y. Bengio, and G. E. Hinton, "Deep learning," *Nature*, vol. 521, pp. 436–444, Dec. 2015.
- [29] V. S. Papanastasiou, R. P. Trommel, R. I. A. Harmanny, and A. Yarovoy, "Deep learning-based identification of human gait by radar micro-Doppler measurements," in *Proc. 17th Eur. Radar Conf. (EuRAD)*, Jan. 2021, pp. 49–52.
- [30] X. Li, Y. He, and X. Jing, "A survey of deep learning-based human activity recognition in radar," *Remote Sens.*, vol. 11, no. 9, p. 1068, May 2019.
- [31] X. Li, Y. He, F. Fioranelli, and X. Jing, "Semisupervised human activity recognition with radar micro-Doppler signatures," *IEEE Trans. Geosci. Remote Sens.*, vol. 60, 2022, Art. no. 5103112.
- [32] C. Wan, L. Wang, and V. V. Phoha, "A survey on gait recognition," ACM Comput. Surv., vol. 51, no. 5, pp. 1–35, Aug. 2018.

- [33] C. Buckley et al., "The role of movement analysis in diagnosing and monitoring neurodegenerative conditions: Insights from gait and postural control," *Brain Sci.*, vol. 9, no. 2, p. 34, Feb. 2019, doi: 10.3390/brainsci9020034.
- [34] A. Middleton, S. L. Fritz, and M. Lusardi, "Walking speed: The functional vital sign," *J. Aging Phys. Activity*, vol. 23, no. 2, pp. 314–322, Apr. 2015.
- [35] C. L. Vaughan, B. L. Davis, and J. C. O'Connor, *Dynamics of Human Gait*. Champaign, IL, USA: Human Kinetics Publishers, 1999.
- [36] J. E. Cutting and L. T. Kozlowski, "Recognizing friends by their walk: Gait perception without familiarity cues," *Bull. Psychonomic Soc.*, vol. 9, no. 5, pp. 353–356, May 1977.
- [37] R. Mc Ardle, S. Del Din, P. Donaghy, B. Galna, A. J. Thomas, and L. Rochester, "The impact of environment on gait assessment: Considerations from real-world gait analysis in dementia subtypes," *Sensors*, vol. 21, no. 3, p. 813, Jan. 2021.
- [38] G. Allali et al., "Gait phenotype from mild cognitive impairment to moderate dementia: Results from the GOOD initiative," *Eur. J. Neurol.*, vol. 23, no. 3, pp. 527–541, Mar. 2016.
- [39] M. S. Nixon and J. N. Carter, "Automatic recognition by gait," *Proc. IEEE*, vol. 94, no. 11, pp. 2013–2024, Nov. 2006.
- [40] L. Z. Gras, S. F. Kanaan, J. M. McDowd, Y. M. Colgrove, J. Burns, and P. S. Pohl, "Balance and gait of adults with very mild Alzheimer disease," *J. Geriatric Phys. Therapy*, vol. 38, no. 1, pp. 1–7, 2015.
- [41] S. Studenski et al., "Gait speed and survival in older adults," J. Amer. Med. Assoc., vol. 305, no. 1, pp. 50–58, 2011.
- [42] V. Valkanova and K. P. Ebmeier, "What can gait tell us about dementia? Review of epidemiological and neuropsychological evidence," *Gait Posture*, vol. 53, pp. 215–223, Mar. 2017.
- [43] F. Pieruccini-Faria et al., "Gait variability across neurodegenerative and cognitive disorders: Results from the Canadian consortium of neurodegeneration in aging (CCNA) and the gait and brain study," *Alzheimer's Dementia*, vol. 17, no. 8, pp. 1317–1328, Feb. 2021.
- [44] A.-M. De Cock et al., "Comprehensive quantitative spatiotemporal gait analysis identifies gait characteristics for early dementia subtyping in community dwelling older adults," *Frontiers Neurol.*, vol. 10, p. 313, Apr. 2019.
- [45] V. Chen, The Micro-Doppler Effect in Radar. Norwood, MA, USA: Artech House, 2011.
- [46] V. C. Chen, "Analysis of radar micro-Doppler with time-frequency transform," in *Proc. 10th IEEE Workshop Stat. Signal Array Process.*, Aug. 2000, pp. 463–466, doi: 10.1109/SSAP.2000.870167.
- [47] R. Boulic, N. M. Thalmann, and D. Thalmann, "A global human walking model with real-time kinematic personification," *Vis. Comput.*, vol. 6, no. 6, pp. 344–358, Nov. 1990.
- [48] S. K. Mitra, Digital Signal Processing: A Computer Based Approach, 1st ed. New York, NY, USA: McGraw-Hill, 1997.
- [49] G. Litjens et al., "A survey on deep learning in medical image analysis," Med. Image Anal., vol. 42, pp. 60–88, Dec. 2017.
- [50] O. Abdel-Hamid, A.-R. Mohamed, H. Jiang, L. Deng, G. Penn, and D. Yu, "Convolutional neural networks for speech recognition," *IEEE/ACM Trans. Audio, Speech Language Process.*, vol. 22, no. 10, pp. 1533–1545, Oct. 2015.
- [51] S. S. R. Phaye, E. Benetos, and Y. Wang, "SubSpectralNet—Using sub-spectrogram based convolutional neural networks for acoustic scene classification," in *Proc. IEEE Int. Conf. Acoust., Speech Signal Process.* (ICASSP), May 2019, pp. 825–829.
- [52] C.-C. Kao, M. Sun, Y. Gao, S. Vitaladevuni, and C. Wang, "Subband convolutional neural networks for small-footprint spoken term classification," in *Proc. Interspeech*, Sep. 2019, pp. 2195–2199.
- [53] N. Takahashi and Y. Mitsufuji, "Multi-scale multi-band densenets for audio source separation," in *Proc. IEEE Workshop Appl. Signal Process.* Audio Acoust. (WASPAA), Oct. 2017, pp. 21–25.
- [54] S. Chang, H. Park, J. Cho, H. Park, S. Yun, and K. Hwang, "Subspectral normalization for neural audio data processing," in *Proc. IEEE Int. Conf. Acoust., Speech Signal Process. (ICASSP)*, Jun. 2021, pp. 850–854.
- [55] K. He, X. Zhang, S. Ren, and J. Sun, "Deep residual learning for image recognition," in *Proc. IEEE Conf. Comput. Vis. Pattern Recognit.* (CVPR), Jun. 2016, pp. 770–778, doi: 10.1109/CVPR.2016.90.
- [56] C. Szegedy et al., "Going deeper with convolutions," in Proc. IEEE Conf. Comput. Vis. Pattern Recognit., Jun. 2015, pp. 1–9, doi: 10.1109/CVPR.2015.7298594.
- [57] D. P. Kingma and J. Ba, "Adam: A method for stochastic optimization," in *Proc. Int. Conf. Learn. Represent.*, 2015, pp. 1–15.
- [58] Z.-H. Zhou, Machine Learning. Berlin, Germany: Springer, 2021.



Fulin Cai received the bachelor's and master's degrees from Shenzhen University, Shenzhen, China, in 2016 and 2019, respectively. He is currently pursuing the Ph.D. degree in computer engineering with Arizona State University, Tempe, AZ, USA.

He was a Research Assistant with the ASU-Mayo Center for Innovative Imaging, Arizona State University, under the supervision of Prof. Teresa Wu. He is particularly interested in leveraging advanced deep learning techniques

to enhance medical applications and improve healthcare outcomes. His current research interests include machine learning, health informatics, and medical sensors.



Abhidnya Patharkar received the bachelor's degree in mechanical engineering and the master's degree in mechanical engineering with a focus on biomechanics from the University of Pune, Pune, India, in 2013 and 2017, respectively. She is pursuing the Ph.D. degree in information management and systems with Arizona State University, Tempe, AZ, USA.

Her focus is on building machine learning models for healthcare applications. Her current research interests include machine learning,

deep learning, and time-series analysis for clinical temporal datasets.



Teresa Wu (Senior Member, IEEE) received the Ph.D. degree in industrial engineering from the University of Iowa, Iowa City, IA, USA, in 2001.

She is a Professor of Industrial Engineering with the School of Computing and Augmented Intelligence, Arizona State University, Tempe, AZ, USA. She has authored more than 140 journal articles, such as IEEE TRANSACTIONS ON BIOMEDICAL ENGINEERING, IEEE JOURNAL OF BIOMEDICAL AND HEALTH INFORMATICS, and Information Science. Her current research interests

include deep learning on heterogenous data, health informatics, and distributed decision support.



Fleming Y. M. Lure received the Ph.D. degree in electrical engineering from Pennsylvania State University, State College, PA, USA, in 1990.

He is a Chief Product Officer with MS Technologies Corporation, Rockville, MD, USA. His research interests include computer-aided detection (CAD), machine learning, and deep learning for disease detection, diagnosis, and prognosis.

Dr. Lure has led a team to receive the first FDA pre-market approved (PMA) early stage

lung cancer detection system on radiograph. He is a member of the Radiological Society of North America (RSNA). He has received more than ten SBIR/STTR Phase I/II awards from NIH and DoD to develop and commercialize computer-aided diagnosis (CAD) systems on lung cancer, tuberculosis, and Alzheimer's diseases on radiological and pathological images deployed worldwide. He also led a team with interdisciplinary backgrounds to annotate large amount of COVID and tuberculosis radiographs to support various government and consortium to provide as high-quality training dataset for artificial intelligence (AI) and clinical researchers worldwide. He is a member of the Radiological Society of North America (RSNA).

Harry Chen received the bachelor's degree in computer science from Oklahoma City University, Oklahoma City, OK, USA, in 1997.

He is currently the Manager of System Development with MS Technologies Corporation, Rockville, MD, USA. He has authored or coauthored five books and more than 180 publications in book chapters, journals, and proceedings. His specialty is integration of large complicated systems involving telephone technology, computer, communication systems for customer relationship management (CRM) with application to automobile vehicle administration, healthcare technology for elderly, and healthcare payment management.

Victor C. Chen (Life Fellow, IEEE) received the Ph.D. degree in electrical engineering from Case Western Reserve University, Cleveland, OH, USA, in 1989.

He was with the Radar Division, U.S. Naval Research Laboratory, Washington, DC, USA, on radar imaging and micro-Doppler effect in radar and retired in 2009.

Dr. Chen is internationally recognized for his work on the micro-Doppler effect in radar and time-frequency-based radar image formation. He often served as a technical program committee member and the session chair for IEEE and other conferences and served as a guest editor for journals. He also served as an Associate Editor for IEEE Transactions on AES from 2004 to 2009.